ORIGINAL ARTICLE

Journal of Cachexia, Sarcopenia and Muscle 2022; **13**: 3163–3180
Published online 13 October 2022 in Wiley Online Library (wileyonlinelibrary.com) **DOI:** 10.1002/jcsm.13106

Atrophic skeletal muscle fibre-derived small extracellular vesicle miR-690 inhibits satellite cell differentiation during ageing

Xiaoyan Shao[1,2], Wang Gong[1,2], Qianjin Wang[1,2], Pu Wang[1,2], Tianshu Shi[1,2], Abdurahman Mahmut[1,2], Jianghui Qin[1,2], Yao Yao[1], Wenjin Yan[1], Dongyang Chen[1], Xiang Chen[1,2]*, Qing Jiang[1,2,3]* & Baosheng Guo[1]*

[1]*State Key Laboratory of Pharmaceutical Biotechnology, Medical School, Nanjing University & Division of Sports Medicine and Adult Reconstructive Surgery, Department of Orthopedic Surgery, Nanjing Drum Tower Hospital, The Affiliated Hospital of Nanjing University Medical School, Nanjing, Jiangsu, China;* [2]*Jiangsu Key Laboratory of Molecular Medicine, Medical School, Nanjing University, Nanjing, Jiangsu, China;* [3]*Laboratory for Bone and Joint Disease, Model Animal Research Center (MARC), Medical School, Nanjing University, Nanjing, Jiangsu, China*

Abstract

Background Sarcopenia is a common and progressive skeletal muscle disorder characterized by atrophic muscle fibres and contractile dysfunction. Accumulating evidence shows that the number and function of satellite cells (SCs) decline and become impaired during ageing, which may contribute to impaired regenerative capacity. A series of myokines/small extracellular vesicles (sEVs) released from muscle fibres regulate metabolism in muscle and extramuscular tissues in an autocrine/paracrine/endocrine manner during muscle atrophy. It is still unclear whether myokines/sEVs derived from muscle fibres can affect satellite cell function during ageing.

Methods Aged mice were used to investigate changes in the myogenic capacity of SCs during ageing-induced muscle atrophy. The effects of atrophic myotube-derived sEVs on satellite cell differentiation were investigated by biochemical methods and immunofluorescence staining. Small RNA sequencing was performed to identify differentially expressed sEV microRNAs (miRNAs) between the control myotubes and atrophic myotubes. The target genes of the miRNA were predicted by bioinformatics analysis and verified by luciferase activity assays. The effects of identified miRNA on the myogenic capacity of SCs in vivo were investigated by intramuscular injection of adeno-associated virus (AAV) to overexpress or silence miRNA in skeletal muscle.

Results Our study showed that the myogenic capacity of SCs was significantly decreased (50%, $n = 6$, $P < 0.001$) in the tibialis anterior muscle of aged mice. We showed that atrophic myotube-derived sEVs inhibited satellite cell differentiation in vitro ($n = 3$, $P < 0.001$) and in vivo (35%, $n = 6$, $P < 0.05$). We also found that *miR-690* was the most highly enriched miRNA among all the screened sEV miRNAs in atrophic myotubes [Log_2 (Fold Change) = 7, $P < 0.001$], which was verified in the atrophic muscle of aged mice (threefold, $n = 6$, $P < 0.001$) and aged men with mean age of 71 ± 5.27 years (2.8-fold, $n = 10$, $P < 0.001$). *MiR-690* can inhibit myogenic capacity of SCs by targeting myocyte enhancer factor 2, including *Mef2a*, *Mef2c* and *Mef2d*, in vitro ($n = 3$, $P < 0.05$) and in vivo ($n = 6$, $P < 0.05$). Specific silencing of *miR-690* in the muscle can promote satellite cell differentiation ($n = 6$, $P < 0.001$) and alleviate muscle atrophy in aged mice ($n = 6$, $P < 0.001$).

Conclusions Our study demonstrated that atrophic muscle fibre-derived sEV *miR-690* may inhibit satellite cell differentiation by targeting myocyte enhancer factor 2 during ageing.

Keywords Sarcopenia; Muscle fibre; Satellite cells; Myogenic capacity; Small extracellular vesicle; *miR-690*

Received: 29 May 2022; Revised: 24 August 2022; Accepted: 2 September 2022
**Correspondence to: Baosheng Guo (lead contact), Qing Jiang and Xiang Chen, State Key Laboratory of Pharmaceutical Biotechnology, Jiangsu Key Laboratory of Molecular Medicine, Medical School, Nanjing University, Nanjing 210093, Jiangsu, China. Email: borisguo@nju.edu.cn*
Qing Jiang, Laboratory for Bone and Joint Disease, Model Animal Research Center (MARC), Medical School, Nanjing University, Nanjing 210093, Jiangsu, China. Email: qingj@nju.edu.cn; chenxiang910110@163.com

Introduction

Sarcopenia is a common and progressive skeletal muscle disorder characterized by loss of muscle mass and impairment of contractile function in the elderly. Currently, the estimates of sarcopenia prevalence vary up to 40.4% depending on the definition used.[1] Sarcopenia seriously reduces mobility and causes fall-related injury, which leads to diminished quality of life, as well as increased morbidity and mortality in elderly people.[2] A systematic review and meta-analysis demonstrated a mortality rate of 3.596% among sarcopenic subjects aged 60 years or older, and even higher in people aged 79 years or older.[3] The age-related muscle atrophy frequently correlates with insufficient levels of muscle regeneration resulting from the impairment of satellite cell activity and myogenesis in the elderly.[4] In addition, satellite cells (SCs) isolated from aged animals also demonstrated a significant lag when entering the cell cycle, decreased differentiation ability and self-renewal.[5] Physiologically, most SCs are maintained in a quiescent, undifferentiated state in the muscle and express a specific *Pax7* marker.[6] Upon muscle injury, quiescent SCs are activated to proliferate, differentiate and fuse with multinuclear myofibres to regenerate muscles.[7] During ageing, the regenerative capacity of SCs can be severely suppressed by endogenous aged environmental factors, including *FGF2*[8] and *IFN-γ*,[9] but the underlying mechanism of SCs dysfunction during ageing-induced muscle atrophy remains elusive.

The skeletal muscle functions as an endocrine organ, in which a series of myokines/small extracellular vesicles (sEVs) are synthesized and released to regulate metabolism in the muscle and extramuscular tissue in an autocrine/paracrine/endocrine manner. Recently, several muscle-derived myokines have been well documented. For instance, myostatin suppresses skeletal muscle growth and causes muscle atrophy, and *IL6* plays a negative role in muscle atrophy,[10] whereas irisin and *FGF21* increase muscle mass.[11,12] In addition to myokines, skeletal muscle fibres also release sEVs into the extracellular milieu to participate in muscle metabolism homoeostasis and the development of skeletal muscle diseases including muscle atrophy.[13] sEVs are 50–150-nm-diameter membranous vesicles play an important role in cell–cell communication by delivering their cargo of various proteins and microRNAs (miRNAs) to target cells and altering their function[14]. Myotube-derived exosomes can promote myoblast differentiation by altering the expression of cyclin D1 and myogenin.[15] MiRNAs encapsulated in sEV are a family of small noncoding RNAs, 20–22 nucleotides in length that directly target the 3′-untranslated region (3′-UTR) of mRNAs and repress gene translation.[16] Studies have confirmed that miRNAs are indeed present in muscle-derived exosomes, and over 170 miRNAs in exosomes derived from C2C12 myoblasts and myotubes have been identified,[17] such as *miR-181a*, *miR-146a*, *miR-378*, *miR-1*, *miR-133a*, *miR-133b* and *miR-206*, which could regulate muscle differentiation. Importantly, several studies have suggested that several pathological events, including injury, atrophy and ageing, can alter the cargo of muscle-derived exosomes.[18] However, the underlying mechanism remains to be elucidated. This study aimed to explore the role of muscle fibre-derived sEVs and their encapsulated miRNAs in modulating satellite cell function during ageing-induced muscle atrophy.

Our study further demonstrated that atrophic muscle fibre-derived sEV *miR-690* inhibits satellite cell differentiation during ageing-induced muscle atrophy. Our findings provide fresh insight into sarcopenia and suggest a potential treatment strategy.

Materials and methods

Animal experiments

The C57BL/6 male mice (age, 8 weeks) were purchased from Nanjing Ziyuan Biotechnology Co. Ltd. (Nanjing, China). The animal experiments were conducted according to the Institutional Animal Ethics Committee and Animal Care Guidelines for the Care and Use of Laboratory Animals of Nanjing University. Three-month-old C57BL/6 mice were served as adult mice, and 24-month-old mice were collected as the aged group. The adeno-associated virus (AAV) loaded with *miR-690* or *miR-690*-sponge recombinase tagged with GFP were synthesized and constructed by Hanheng Biotechnology Co., Ltd. (Shanghai, China). The TA muscles of mice were injected with 30 μl AAV (10^{12}), and the TA muscles were collected for further investigation 1-month post-injection.

Cell culture and transfection

Mouse C2C12 myoblasts and human HEK293T cells were obtained from ATCC and cultured in DMEM containing 10% foetal bovine serum (FBS, Gibco) and 1% penicillin–streptomycin under 5% CO_2 and 37°C. For the myogenic differentiation experiment, when confluence was reached to 80–90%, myoblasts were induced with differentiation medium-DMEM containing 2% horse serum (Hyclone). For miRNAs or siRNA transfection, C2C12 myoblasts were seeded into 12-well or 6-well plates and reached to 70–80% confluency. Then C2C12 myoblasts were transfected with either *miR-690* mimics (Ribo, Guangzhou, China) at 50 nmol/mL, *miR-690* inhibitors (Ribo, Guangzhou, China) at 100 nmol/mL, si-Mef2c (Generay Biotech, Shanghai, China) at 100 nmol/mL or negative control using Lipofectamine 2000 (Invitrogen, Guangzhou, China). After 6–8 h, the culture medium was replaced with differentiation medium, and the cells were incubated for 5 days. The 293T cells were used for the luciferase reporter assays. The synthesized siRNA sequences

for inhibition of Mef2c are 5′-GCATTGAACAAGAAAGAAA-3′ (Generay biotech, Shanghai, China). For co-culture and transfection experiments, C2C12 cells were seeded into the well inserts with a 0.4-μm pore-sized filter (Corning Inc., USA) and differentiated into myotubes. C2C12 myoblast cells were seeded into 6-well plates. Myotubes were transfected with the lentiviral CMV-GFP-CD63 lentiviral vector (GFP-CD63)/ negative control lentivirus (NC) (Jikai Gene, China) at a multiplicity of infection (MOI) of 100. After 24 h, the medium was replaced, and the myotubes were induced to atrophy. And then the atrophic myotubes were co-culture with myoblast for 48 h.

Human species

The study of human specimens has been approved by the Medical Ethics Committee of the Affiliate Drum Tower Hospital, Medical School of Nanjing University in accordance with the Declaration of Helsinki (2020-323-01). All participants gave written informed consent. All subjects analysed were adult men (31 ± 7.73 years, n = 9) or aged men (71 ± 5.27 years, n = 10), which exclude any metabolic diseases, liver/renal diseases or inflammatory diseases. Muscle specimens were collected from gluteus medius of participants during surgery. The information of all subjects was shown in *Table* S1.

Physiologic muscle force generation assay

Muscle force generation capacity was analysed in EDL muscles using an ASI muscle contraction system (Aurora Scientific). Mice were maintained under isoflurane throughout the procedure. TA was removed, and EDL were dissected, adjusted to optimal length (OL) and tested at different frequencies to determine absolute force values. Muscle force was recorded and analysed using Dynamic Muscle Control and GraphPad Prism software.

Immunofluorescence staining

For immunofluorescence, fresh TA muscles dissected from mice were collected and immediately fixed in ice-cold 4% paraformaldehyde solution overnight, and infiltration was followed with a mixture of 30% sucrose phosphate buffer for 1 day. All samples were snap-frozen in optimum cutting temperature (O.C.T., Fisher Healthcare) with dry ice and cut into 5-μm-thick cross sections using a cryostat. Immunofluorescence staining was performed as described[9] and hybridized overnight with primary antibodies (listed in *Table* S3) and with the appropriate secondary antibodies (Invitrogen, Guangzhou, China). Nuclei were counterstained with DAPI (Beyotime, China).

Western blotting and antibodies

The cells or sEVs were homogenized and lysed in RIPA buffer supplemented with protease and phosphatase inhibitors (Thermo Fisher Scientific, USA). Protein concentrations were quantified using a BCA Protein Assay Kit (Beyotime, Nanjing, China). Total proteins were boiled at 95°C for 5 min after adding the 5× SDS-PAGE protein loading buffer (BOSTER, China). After electrophoresis on 7.5% or 10% SDS-PAGE gels, proteins were transferred to PVDF membranes (Bio-Rad, CA) and incubated with the primary antibodies. The antibodies were listed in *Table* S3. The membranes were further incubated with HRP-conjugated secondary antibodies (Proteintech, China), and an ECL Western Blotting Substrate Kit (Tanon, China) was then used to visualize signals.

sEV isolation, characterization and in vivo trafficking assays

To isolate sEVs, C2C12 cells were cultured in DMEM containing 10% sEV-depleted FBS (Gibco) or EBSS; then the supernatants of cells were collected, and sEVs extracted using ultracentrifugation. The final pellet was resuspended in PBS, and protein concentration was measured by BCA (Beyotime, Nanjing, China). Interstitial sEVs were isolated by adapting a recently described protocol.[19] Muscle tissues used to isolate interstitial sEVs were rinsed well with PBS; then the muscle tissues were minced and digested for 1 h at 37°C in buffer containing 100 mM HEPES, 1.5% BSA, 5 mM glucose, 1 mM calcium and 1 mg/mL collagenase II. After dilution in PBS and 2 mM EGTA to inhibit collagenase activity, sEVs were extracted using ultracentrifugation, and then the pelleted sEVs were resuspended in PBS. The sEV size was measured by dynamic light scattering (ZEN3600 Zetasizer, Malvern, UK). For transmission electron microscopy (TEM), 5 μL of sEV sample solution was transferred to formvar and carbon-coated copper grids. The grids were covered and incubated for 10 min before they were stained with 1% uranyl acetate. Western blotting was used to identify the expression of EV-specific proteins (CD81, CD9). For sEV-tracing experiments, the PKH26 Red Fluorescent Cell Linker Kit for General Cell Membrane Labelling (Sigma-Aldrich) was used according to the manufacturer's instructions and diluted in PBS, which were injected to the TA muscles of adult mice. Twelve hours after sEVs injection, TA muscles were collected for further detecting.

In vivo and in vitro sEVs and GW4869 treatment

In vitro, sEVs (20 μg/mL) were co-cultured with C2C12 cells for 5 days from differentiating, and the culture medium containing sEVs was changed every 2 days. In vivo, 20 μL PBS

containing 100 μg of sEVs was intramuscularly injected into TA muscle twice per week. GW4869 (Sigma-Aldrich) was dissolved in DMSO to a concentration of 0.1 mg/μL as a stock solution, and the stock solution was dissolved in 0.9% normal saline at 0.1 μg/μL for the experiment. The TA muscles of aged mice were intramuscularly injected with 50 μL of PBS (0.1% DMSO) or GW4869 per other day for 14 days.

RNA extraction, reverse transcription and real-time quantitative PCR

Total RNA from TA muscles or C2C12 cells was extracted with TRIzol reagent (Invitrogen, Life Technologies) according to the manufacturer's instructions. The expression of mature miRNAs was detected by a Hairpin-it miRNA and U6 snRNA normalization Q-PCR Quantitation Kit (Ribo, Guangzhou, China), and the primers for miRNAs were obtained from Ribo (Guangzhou, China). sEV RNA was isolated using an miRNeasy kit (QIAGEN Sciences, Maryland, MD), and when isolating RNA from 100 μg sEVs, a spike-in control miRNA (cel-miR-39-3p) was added as an extraction normalization control. Real-time qPCR was performed with the ChamQ SYBR qPCR Master Mix (Vazyme, Nanjing, China). The primer sequences used are shown in *Table* S2.

Luciferase reporter assays

Luciferase reporter plasmids (psiCHECK2) containing the WT or mutant 3'-UTR of Mef2c, Mef2a and Mef2d were manufactured by Hanheng Biotechnology (Shanghai, China).

Small RNA deep sequencing and bioinformatics analysis

MiRNA components in either control myotubes-sEVs or atrophic myotubes-sEVs were profiled by single-end sequencing (1 × 50 bp) on an Illumina platform (NEB, USA) at Novogene (Beijing, China). The raw data were processed through custom perl and python scripts and subsequently aligned to all mouse miRNA mature and hairpin sequences in release 20.0 of miRBase. The small RNA tags were mapped to reference sequence by Bowtie (Langmead et al., 2009) without mismatch to analyse their expression and distribution on the reference. Differential expression analysis of two conditions/groups was performed using the DESeq R package (3.0.3). The *P* values was adjusted using the Benjamini and Hochberg method. Corrected *P* value of 0.05 was set as the threshold for significantly differential expression by default. Sequencing data supporting these studies can be found at the Gene Expression Omnibus database under accession number (GSE211885).

Statistics analysis

Data are presented as means ± SEM. Statistical analysis was performed using unpaired Student's *t*-tests or one-way ANOVA. Statistical analyses were performed with GraphPad Prism software (version 8.0.1). *P* values < 0.05 were considered to be statistically significant.

Results

The myogenic capacity of SCs decreased in company with muscle atrophy in aged mice

To investigate the changes in muscle fibre morphology, contractile function and myogenic capacity of SCs in skeletal muscle during ageing-induced muscle atrophy, we employed a natural ageing mouse model in our study, that is, 24-month-old wild-type mice with 10–20% grey hair indicating depigmentation of the cloth.[20] First, we observed decreased fibre cross-sectional area (fCSA) of tibialis anterior (TA) muscles (*Figure* 1A) as well as elevated expression levels of muscle atrophy-related genes including atrogin-1 and murf-1 (*Figure* 1B) in aged mice (24-month-old mice) compared with those in adult mice (3-month-old mice). We also examined the changes in contractile function of skeletal muscle during ageing and found decreased maximal tetanic force of the extensor digitorum longus (EDL) in aged mice compared with that in adult mice (*Figure* 1C). As it was reported that the number pool of SCs decreases during ageing, we further quantified the total number of SCs, as indicated by *Pax7*-positive staining, a critical transcription factor for maintaining SCs function and expressed in both quiescent and activated SCs.[6] Consistent with previous studies, the results revealed that the number of $Pax7^+$ SCs was dramatically reduced in the TA muscle of aged mice relative to that in adult mice (*Figure* 1D). As activated SCs start to express *MyoD*, $Pax7^+/MyoD^+$ SCs have been used to represent SCs in transit towards differentiation, we performed co-immunofluorescence staining of *Pax7* with *MyoD* for subsequent semi-quantitative analysis. Indeed, the number of $Pax7^+/MyoD^+$ cells was significantly reduced in the TA muscle of aged mice compared with that in adult mice (*Figure* 1E). Thus, these results suggest that the impaired myogenic capacity of SCs occurs in conjunction with muscle fibre atrophy and contractile dysfunction during ageing.

sEVs released from atrophic myotubes inhibited myoblast differentiation in vitro

To further explore the effect of atrophic myotubes on myoblast differentiation, we constructed a starvation-induced

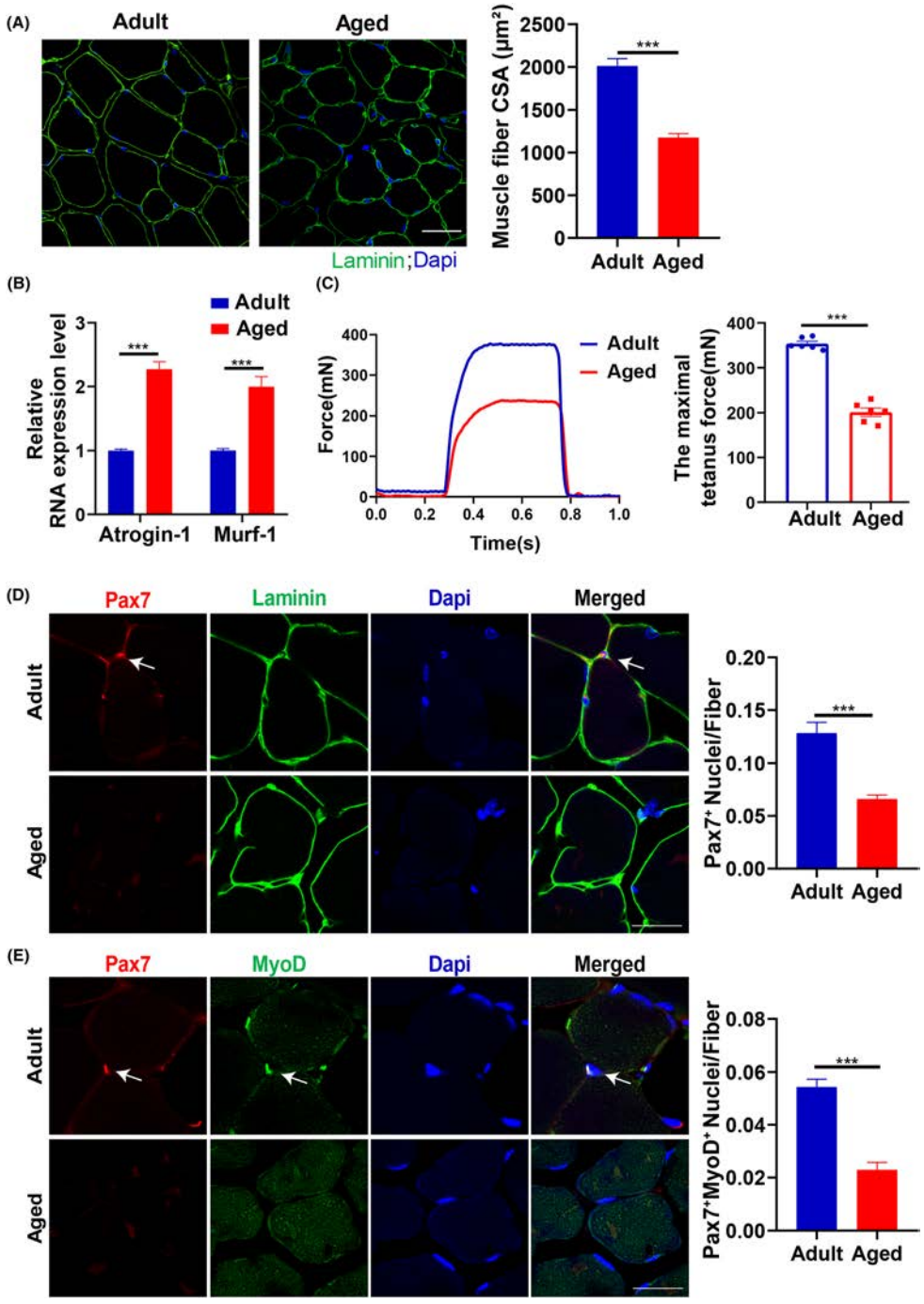

Figure 1 The myogenic capacity of SCs decreased in company with muscle atrophy in aged mice. (A) Left panel: The representative images of immunofluorescent staining for fibre cross section in TA muscle from adult mice and aged mice. The muscle fibre membranes were immunostained with anti-laminin antibody (green) and the nuclei in muscle fibres were labelled with Dapi (blue). Scale bars, 100 μm. Right panel: The semi-quantitative analysis of fCSA for TA from adult mice and aged mice. (B) Q-PCR analysis of Atrogin-1 and Murf-1 mRNA levels in TA muscles from adult mice and aged mice. (C) Left panel, the representative curve for tetanic force generated during tetanic stimulation in EDL from adult and aged mice. Right panel, the maximal tetanic force in EDL from adult and aged mice. (D) Left panel, the representative images of immunofluorescent staining for Pax7 (red) and laminin (green) in TA muscle sections from adult mice and aged mice. The nuclei were labelled with DAPI (blue). Scale bars: 50 μm. Right panel: The average number of Pax7 positive staining SCs ($Pax7^+$) per TA section of adult mice and aged mice. (E) Left panel: The representative images of immunofluorescent staining for Pax7 (red) and MyoD (green) in TA section from adult mice and aged mice. Nuclei were labelled with DAPI (blue). Scale bars, 50 μm. Right panel: The average number of double-positive staining with $Pax7^+$ and $MyoD^+$ SCs ($Pax7^+/MyoD^+$) per TA section of adult mice and aged mice. Notes: Data are presented as means ± SEM. $^*P < 0.05$, $^{**}P < 0.01$, $^{***}P < 0.001$ by Student's *t*-test. *N* = 6 for each group. EDL, extensor digitorum longus; fCSA, muscle fibre cross-sectional area; SCs, satellite cells; TA, tibialis anterior.

DOI: 10.1002/jcsm.13106

myotube atrophy model in vitro. We found reduced myotube diameter (*Figure* S1A) and elevated expression levels of muscle atrophy-related genes, including atrogin-1 and murf-1 (*Figure* S1B) after starvation induction in Earle's balanced salt solution (EBSS) for 7 h. Previous studies have shown that skeletal muscle can release sEVs to exert important paracrine/autocrine actions on muscle metabolism[13]; therefore, we speculated that sEVs released from atrophic myotubes could affect the myogenic capacity of SCs that reside beneath the basal lamina surrounding muscle fibres. To test this hypothesis, we identified and isolated sEVs secreted by myotubes during starvation-induced atrophy and investigated their effects on the regenerative capacity of SCs. Representative cryogenic electron microscopy (cryo-EM) confirmed that the sEVs in the supernatant released from starvation-induced atrophic myotubes appeared as round vesicles delimited by an intact, dense outer wall and a less dense inner region, with a mean diameter of approximately 70 nm (*Figure* 2A). Dynamic light scattering (DLS) demonstrated that the particle size distribution of sEVs in the supernatant of starvation-induced atrophic myotubes was 106 ± 5 nm (*Figure* 2B). Furthermore, western blot analysis also showed that CD81 and CD9, two well-defined EV markers highly expressed in sEVs, whereas calnexin, a marker of the endoplasmic reticulum, did not exist in sEVs (*Figure* 2C). To verify whether sEVs were transferred from atrophic myotubes to myoblasts, we constructed a lentiviral system of cytomegalovirus (CMV)-driven green fluorescence protein (GFP)-tagged CD63 (CMV-GFP-CD63) to label sEVs derived from atrophic myotubes. Subsequently, the atrophic myotubes were co-cultured with C2C12 myoblasts for 48 h, and we observed numerous GFP^+ particles within C2C12 myoblasts by confocal imaging (*Figure* S1C). C2C12 myoblasts were then incubated with sEVs (20 μg/mL) released from atrophic myotubes (ATR-sEVs) and control myotubes (CON-sEVs), respectively. Immunofluorescence staining of MYHC demonstrated that C2C12 myoblasts incubated with ATR-sEVs presented fewer myotubes than those co-cultured with CON-sEVs (*Figure* 2D). Consistently, incubation with ATR-sEVs also markedly suppressed the mRNA (*Figure* 2E) and protein (*Figure* 2F) expression levels of myogenesis-related genes, including *Myod*, *Myog* and *Myhc*, in C2C12 myoblasts during differentiation. Altogether, these data suggest that sEVs released from atrophic myotubes can inhibit myoblast differentiation in vitro.

sEVs released from atrophic myotubes inhibited SCs differentiation in vivo

To investigate whether sEVs released from atrophic myotubes could influence the activity of SCs in vivo, we purified CON-sEVs/ATR-sEVs and administered them to adult mice

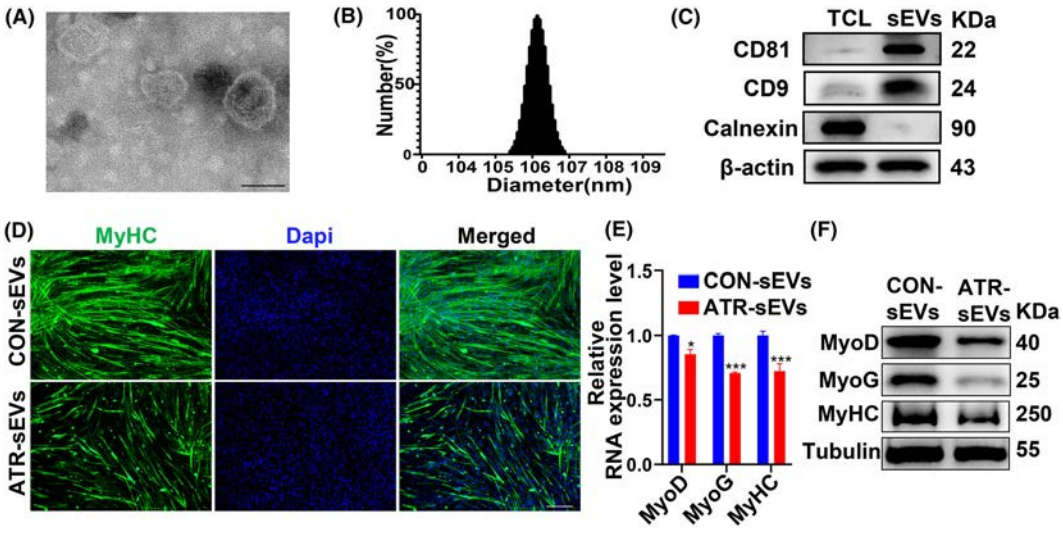

Figure 2 sEVs released from atrophic myotube inhibited myoblast differentiation in vitro. (A) The representative cryo-EM images of sEVs in supernatant released from starvation-induced atrophic myotubes. Scale bar, 50 nm. (B) Dynamic light scattering (DLS) showing the particle size distribution of sEVs in supernatant from atrophic myotubes induced by starvation. (C) Western blot analysis for the protein expression of the EV markers (CD81 and CD9) in both sEVs in supernatant and total cell lysate (TCL) from atrophic myotubes. The sEVs fraction is missing the ER marker (calnexin), whereas the TCL fraction is free from the sEVs markers (CD81 and CD9). (D) The representative images of immunofluorescence staining for MyHC in C2C12 myoblasts during differentiation after treated with sEVs released from atrophic and control myotubes, respectively. Scale bars, 200 μm. (E) Q-PCR analysis for the mRNA expression levels of myogenesis-related genes, including *MyoD*, *MyoG* and *MyHC*, in C2C12 myoblast during differentiation after incubation with sEVs released from atrophic and control myotubes, respectively. (F) Western blot analysis for the protein levels of myogenesis-related genes in C2C12 myoblasts during differentiation after adding CON-sEVs and ATR-sEVs, respectively. Notes: Data are presented as means ± SEM. $^*P < 0.05$, $^{**}P < 0.01$, $^{***}P < 0.001$ by Student's *t*-test. $N = 3$ for the group (D, E). ATR-sEVs, sEVs from atrophic myotubes; CON-sEVs, sEVs from control myotubes; cryo-EM, cryogenic electron microscope; DLS, dynamic light scattering; ER, endoplasmic reticulum; TCL, total cell lysate.

DOI: 10.1002/jcsm.13106

via intramuscular injection (i.m., 100 μg) into the TA muscle once every other day for 14 days (*Figure* 3A). We found that CON-sEVs and ATR-sEVs can enter muscle satellite cells by labelling EVs with PKH26 (*Figure* 3B). The results revealed that the number of $Pax7^+$ SCs in the TA muscle of ATR-sEVs-treated mice was lower than that in CON-sEVs-treated mice (*Figure* 3C). Double immunofluorescence labelling of *Pax7* with *MyoD* also demonstrated that the number of $Pax7^+MyoD^+$ cells in the TA muscle of ATR-sEVs-treated mice was significantly reduced compared with that in CON-sEVs-treated mice (*Figure* 3D). These results suggest that atrophic myotube-derived sEVs directly inhibit satellite cell differentiation in vivo.

Blockage of sEV generation in atrophic muscle by GW4869 improved SC myogenic capacity in aged mice

To further investigate whether the blockage of sEV generation from muscle fibres could affect satellite cell differentiation, a sEV inhibitor (GW4869) was used to block sEV generation in muscle fibres (*Figure* 4A and 4B). The immunofluorescence results showed that the number of $Pax7^+$ SCs (*Figure* 4C) and $Pax7^+MyoD^+$ cells (*Figure* 4D) were significantly increased in the TA muscle of GW4869 treatment aged mice. Interestingly, GW4869 treatment effectively enhanced fibre CSA in aged mice (*Figure* S2A). The EDL muscle in GW4869 treatment mice also generated a significantly higher maximal force than that in the control mice (*Figure* S2B). Moreover, the expression of muscle atrophy-related genes atrogin-1 and murf-1 was significantly decreased in GW4869 treatment mice (*Figure* S2C). These data indicate that blocking sEV generation from myofibres could improve SCs myogenic capacity and alleviate muscle atrophy during ageing.

MiR-690 highly enriched in sEVs released from atrophic myotubes and muscles induced by ageing

To identify differentially expressed miRNAs in sEVs released from myotubes during atrophy, we performed deep sequencing of small RNAs in sEVs released from control and atrophic myotubes. A volcano plot of differentially enriched miRNAs showed 45 up-regulated miRNAs and 58 down-regulated miRNAs with statistical significance ($P < 0.05$) in the sEVs released from atrophic myotubes compared with sEVs released from control myotubes (*Figure* 5A and 5B). Among the up-regulated miRNAs, *miR-690* was identified as the most enriched miRNA in sEVs released from myotubes during myotube atrophy. Consistent with the findings of RNA sequencing, we also detected by Q-PCR analysis that *miR-690* levels in sEVs released from atrophic myotubes were markedly higher than those in sEVs released from control myotubes (*Figure* 5C). Consistently, *miR-690* expression in atrophic myotubes was also significantly higher than that in control myotubes (*Figure* 5D). In addition, we further confirmed that *miR-690* expression level in the TA tissue of aged mice was significantly increased compared with those in adult mice (*Figure* 5E). More importantly, the *miR-690* expression level in the muscle tissue of aged humans was also obviously higher than that of adult humans **(***Figure* 5F**)**. Collectively, *miR-690* was identified as the most enriched miRNA in sEVs released from ageing-induced atrophic myotubes and muscles.

MiR-690 inhibited C2C12 myoblast differentiation by targeting myocyte enhancer factor 2 including Mef2a, Mef2c and Mef2d in vitro

To explore the functional role of sEV *miR-690* in myogenic differentiation, C2C12 myoblasts were transfected with *miR-690* mimics, *miR-690* inhibitors and a negative control (NC) with 80% transfection efficiency and subsequently induced to differentiate. The results showed that the expression of *miR-690* in myotubes was dramatically up-regulated or down-regulated after transfection with *miR-690* mimics or inhibitors, respectively (*Figure* 6A). Immunofluorescence staining of MYHC demonstrated that myoblasts presented fewer myotubes and a reduced fusion rate after transfection with *miR-690* mimics, whereas the number of myotubes and fusion rate increased after miR-690 inhibitor treatment when compared with the NC group (*Figure* 6B). Overexpression of *miR-690* using miR-690 mimics markedly suppressed the mRNA and protein expression levels of myogenesis-related genes, including MyoD, MyoG and MyHC in myoblasts (*Figure* 6C). In contrast, *miR-690* inhibitor transfection significantly increased the mRNA and protein expression levels of these myogenesis-related genes (*Figure* 6C). These results indicated that *miR-690* could inhibit C2C12 myoblast differentiation and suppress the expression of myogenesis-related genes.

Despite the inhibitory effects of *miR-690* on myoblast differentiation, the underlying regulatory mechanisms and their target genes remain unknown. To identify and validate the target genes of *miR-690*, we used several online miRNA target gene prediction tools (TargetScan and miRmap) to predict its potential regulatory target genes. Among the predicted targets, *Mef2c* plays an important role in myogenesis and possesses two potential binding sequences for *miR-690* in the 3′-UTR region. To validate whether these two binding sequences were responsible for the interaction between *Mef2c* and *miR-690*, we mutated binding sequence 1 (Mut1), binding sequence 2 (Mut2) or both (Mut1/2) for subsequent experiments (*Figure* 6D). Next, we subcloned wild-type (WT) *Mef2c* or mutant *Mef2c* (Mut1, Mut2 or Mut1/2) into the psiCHECK™-2 vector and subsequently performed luciferase

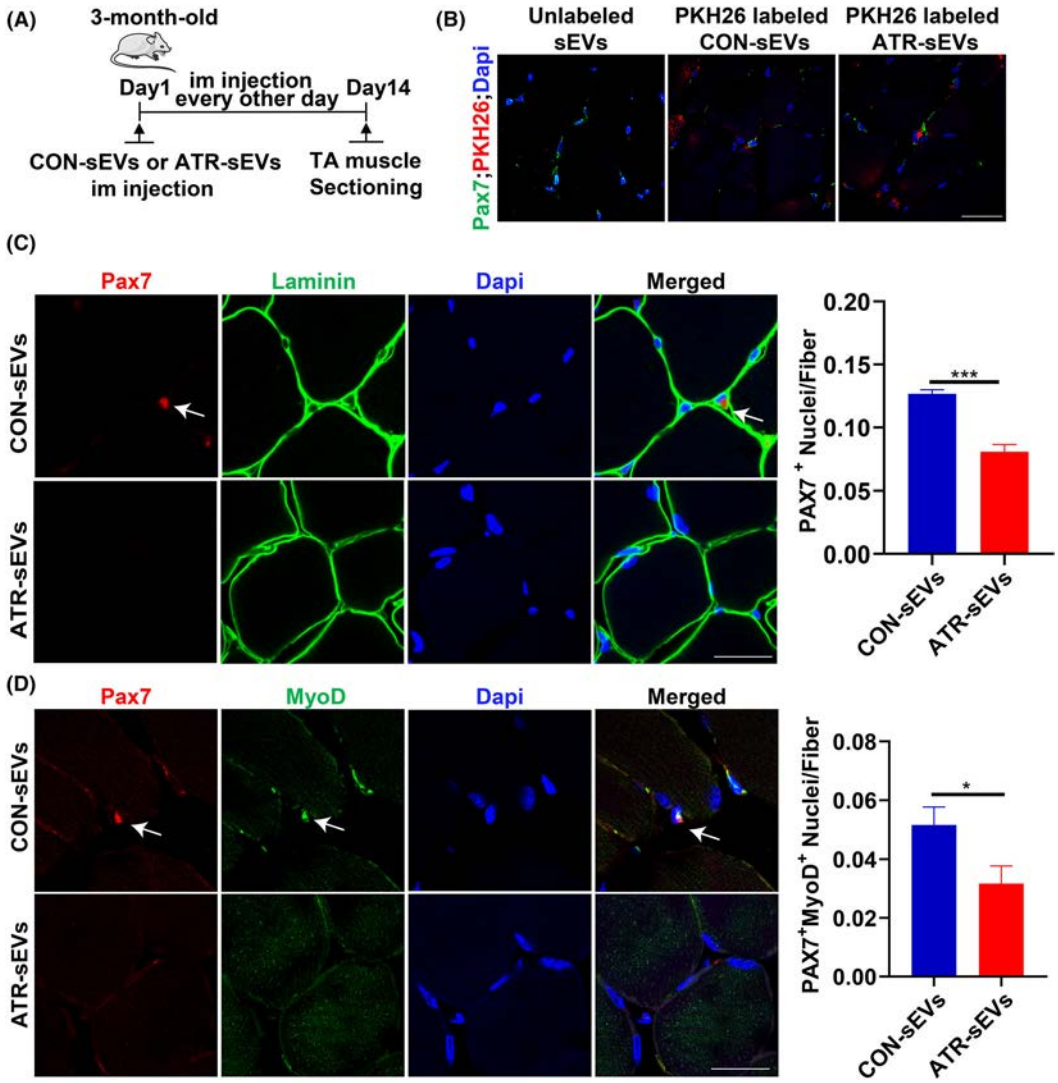

Figure 3 sEVs released from atrophic myotube inhibited myoblast differentiation in vivo. (A) Schematic diagram showing the experimental design for administration adult mice ATR-sEVs and CON-sEVs via intramuscular injection (i.m., 100 μg) into TA muscle once every other day for 14 days. (B) The representative images of immunofluorescent staining for PKH26 (red) and Pax7 (green) in TA muscle sections of adult mice 12 h after intramuscular injection with unlabelled sEVs (left), PKH26-labelled CON-sEVs (middle), PKH26-labelled ATR-sEVs (right). Nuclei were co-stained with Dapi (blue). Scale bars, 100 μm. (C) Left panel: The representative images of immunofluorescent staining for Pax7 (red) and laminin (green) in TA muscle sections from CON-sEVs treated mice and ATR-sEVs treated mice. The nuclei were labelled by Dapi (blue). Scale bars: 50 μm. Right panel: The average number of Pax7 positive staining SCs ($Pax7^+$) per TA section of CON-sEVs treated mice and ATR-sEVs treated mice. ***(D)*** *Left panel,* the representative images of immunofluorescent staining for Pax7 (red) and MyoD (green) in TA section from mice treated with CON-sEVs and ATR-sEVs, respectively. Nuclei were labelled with Dapi (blue). Scale bars, 50 μm. Right panel: The average number of double positive labelling with Pax7 and MyoD cells ($Pax7^+MyoD^+$) in TA section from mice treated with CON-sEVs and ATR-sEVs, respectively. Notes: Data are presented as means ± SEM. $^*P < 0.05$, $^{**}P < 0.01$, $^{***}P < 0.001$ by Student's *t*-test. *N* = 6 for mice group (C, D). ATR-sEVs, sEVs from atrophic myotubes; CON-sEVs, sEVs from control myotubes; TA, tibialis anterior.

reporter assays in HEK293T cells. Dual-luciferase reporter assays showed that *miR-690* mimics directly repressed the luciferase activity of the WT and Mut2 reporters, but not that of the Mut1 reporter and Mut1/Mut2 reporter (*Figure* 6D), indicating that binding sequence 1 was responsible for the interaction of *Mef2c* and *miR-690*. These results revealed that *miR-690* directly interacted with binding sequence 1 at the 3′-UTR region of *Mef2c*. *Mef2c* is a member of the myocyte enhancer factor-2 (*MEF2*) family of transcription factors, and other members including *Mef2a* and *Mef2d* also play important roles in muscle differentiation. In addition, we found that *miR-690* exhibited an identical binding sequence to the seed region sequences of *Mef2a, Mef2d* and *Mef2c* mRNAs. It is likely that *miR-690* targets *Mef2a* and *Mef2d* genes. The dual-luciferase reporter assay confirmed these binding effects (*Figure*

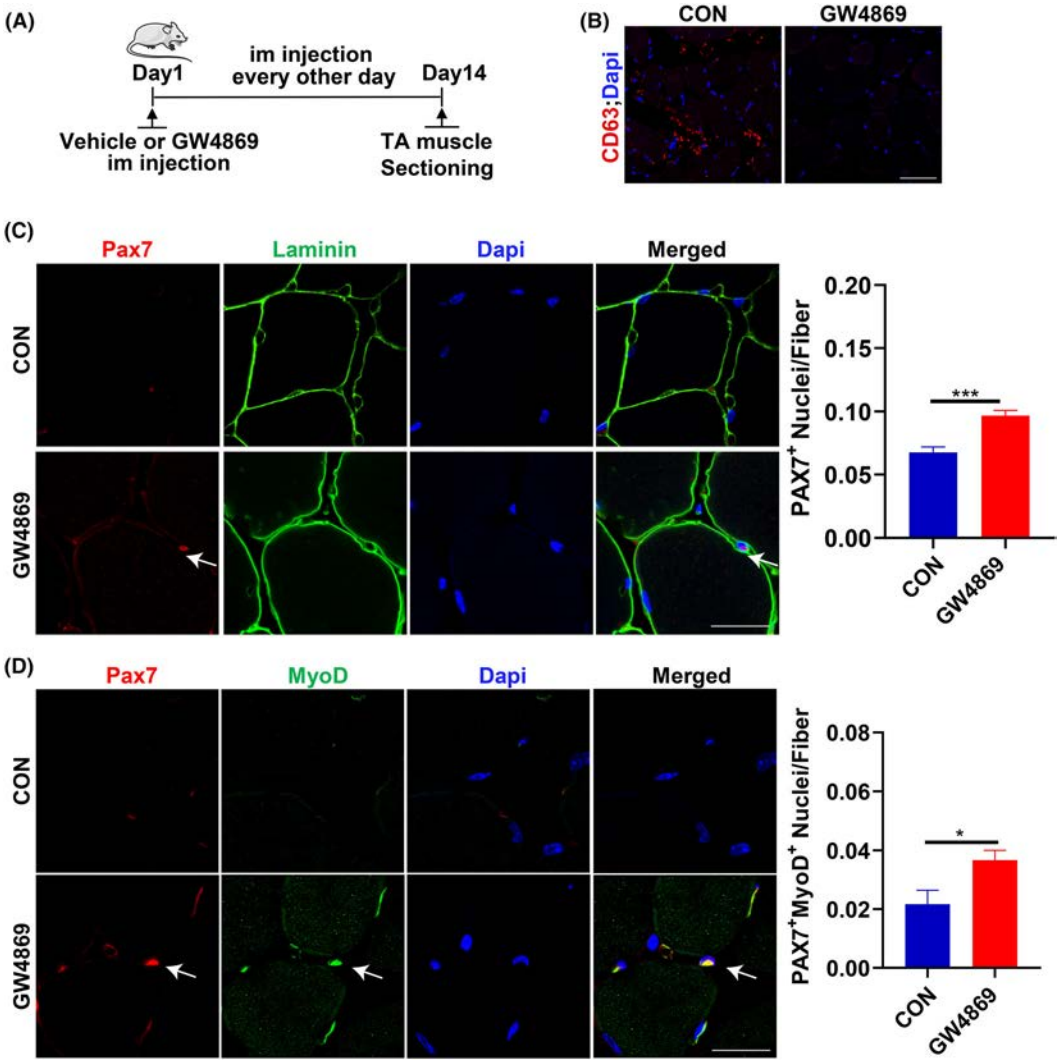

Figure 4 Blockage of sEV generation in atrophic muscle by GW4869 promoted SCs myogenic capacity in aged mice. (A) Schematic diagram illustrating the experimental design of administrating aged mice with GW4869 via daily intramuscular injection for 14 days. (B) The representative images of immunofluorescent staining for CD63 (red) in TA section from aged mice injected with PBS (control) and GW4869, respectively. Nuclei were co-stained with Dapi (blue). Scale bars, 100 μm. (C) Left panel: The representative images of immunofluorescent staining for Pax7 (red) and laminin (green) in TA muscle sections from aged mice after intramuscular injection of PBS (control) and GW4869, respectively. The nuclei were labelled by Dapi (blue). Scale bars: 50 μm. Right panel: The average number of Pax7 positive staining SCs ($Pax7^+$) per TA section of control mice and GW4869 injected mice. (D) Left panel: The representative images of immunofluorescent staining for Pax7 (red) and MyoD (green) in TA section from aged mice after intramuscular injection of PBS (control) and GW4869, respectively. Nuclei were labelled with Dapi (blue). Scale bars, 50 μm. Right panel: The average number of $Pax7^+$ $MyoD^+$ cells per TA section of control mice and GW4869 injected mice. Notes: Data are presented as means ± SEM. $^*P < 0.05$, $^{**}P < 0.01$, $^{***}P < 0.001$ by Student's *t*-test. $N = 6$ for mice group (C, D). TA, tibialis anterior.

S3A–S3D). We then manipulated the expression of *miR-690* in myoblasts by transfection with either *miR-690* mimics or inhibitors and observed that overexpression of *miR-690* by *miR-690* mimics strongly repressed *Mef2a* and *Mef2d* expression, whereas inhibition of *miR-690* by miR-690 inhibitors significantly increased the expression of *Mef2a* and *Mef2d* (*Figure* S3E and S3F).

Furthermore, we examined the expression of *miR-690* and *Mef2c* during C2C12 myoblast differentiation. The results showed that the expression level of *miR-690* gradually decreased, but that of *Mef2c* decreased during myoblast differentiation (*Figure S4A–S4C*). Because *miR-690* could inhibit myoblast differentiation and *Mef2c* was validated as its target gene, we hypothesized that *miR-690* might inhibit myoblast differentiation by targeting *Mef2c*. To verify our hypothesis, we manipulated the expression of *miR-690* in myoblasts by transfection with either *miR-690* mimics or inhibitors and observed that overexpression of *miR-690* by *miR-690* mimics strongly repressed *Mef2c* expression, whereas inhibition of *miR-690* by *miR-690* inhibitors significantly increased the

DOI: 10.1002/jcsm.13106

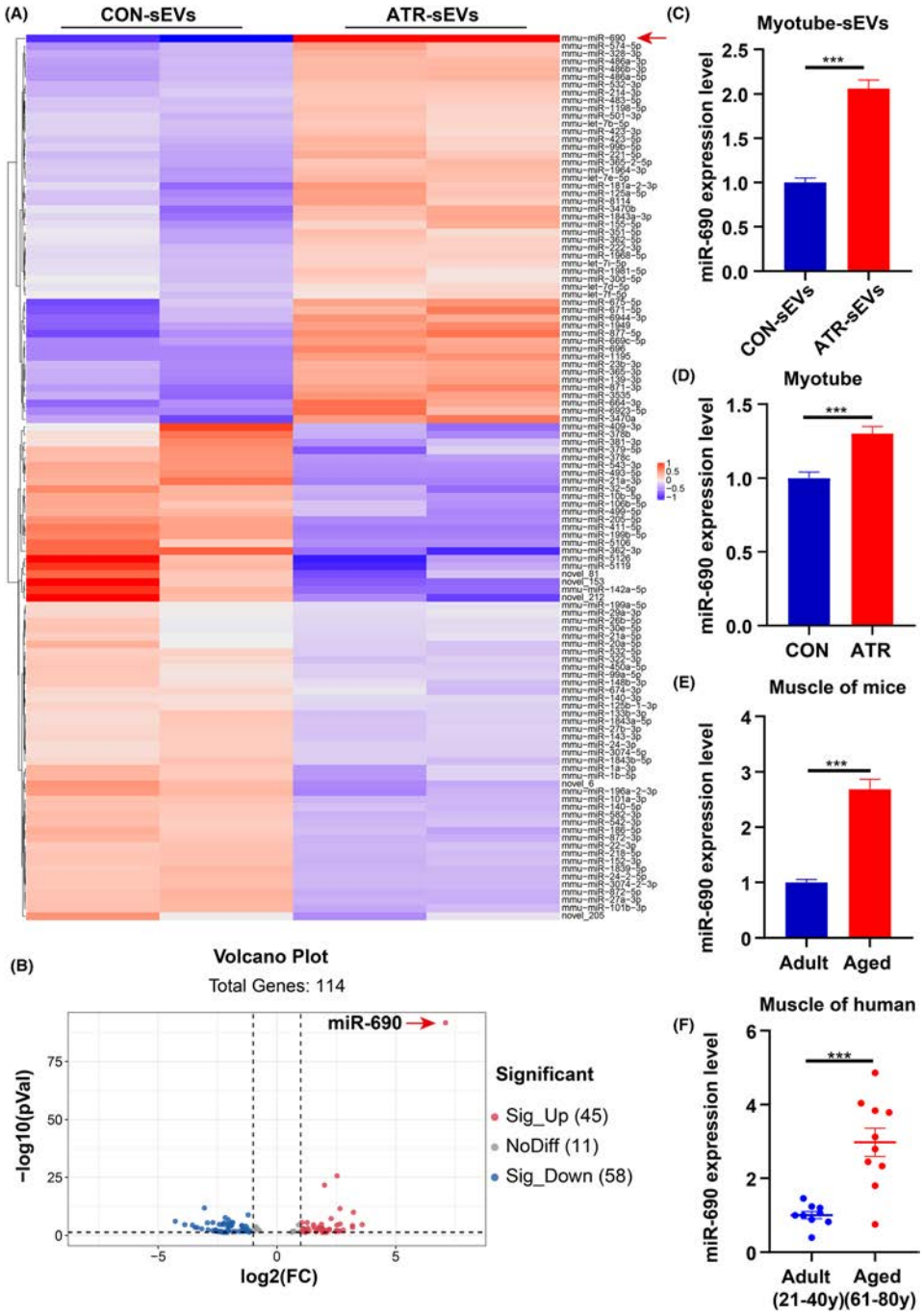

Figure 5 *MiR-690* enriched in sEVs released from atrophic myotubes and muscles induced by ageing. (A) Volcano plot of differentially enriched miRNAs showing 45 up-regulated miRNAs and 53 down-regulated miRNAs in the sEVs released from atrophic myotubes compared with those sEVs secreted from control myotubes [Log_2(fold change) > 2]. The scattered dots indicate the individual miRNAs, the grey dots represent the miRNAs with no significant difference, the red dots represent the significantly up-regulated differential miRNAs, and the blue dots represent the significantly down-regulated differential miRNAs. *MiR-690* is the mostly enriched sEV miRNA among all the up-regulated miRNAs. (B) Hierarchical clustering and heat map of the changed miRNAs. Scale bars show mean-centred log2 normalized counts (row Z score), where red and blue column boxes indicate higher and lower than mean abundance, respectively. Each column represents a different sample and rows represent miRNA transcripts. (C) Q-PCR analysis of *miR-690* expression level in CON-sEVs and ATR-sEVs, respectively. (D) Q-PCR analysis of *miR-690* expression level in control myotubes (CON) and atrophic myotubes (ATR), respectively. (E) Q-PCR analysis of *miR-690* expression level in TA muscle from adult mice and aged mice, respectively. (F) Q-PCR analysis of *miR-690* expression level in muscle tissue from adult human (21–40 years) and aged human (61–85 years), respectively. Notes: The data are expressed as mean ± SEM; $n = 6$ mice for mice group (E), $n = 3$ for the other group (C, D) and $n = 9$ for adult human group, $n = 10$ for aged human group. $^*P < 0.05$, $^{**}P < 0.01$, $^{***}P < 0.001$ by Student's *t*-test. ATR, atrophic myotubes; ATR-sEVs, sEVs from atrophic myotubes; CON, control myotubes; CON-sEVs, sEVs from control myotubes; TA, tibialis anterior.

DOI: 10.1002/jcsm.13106

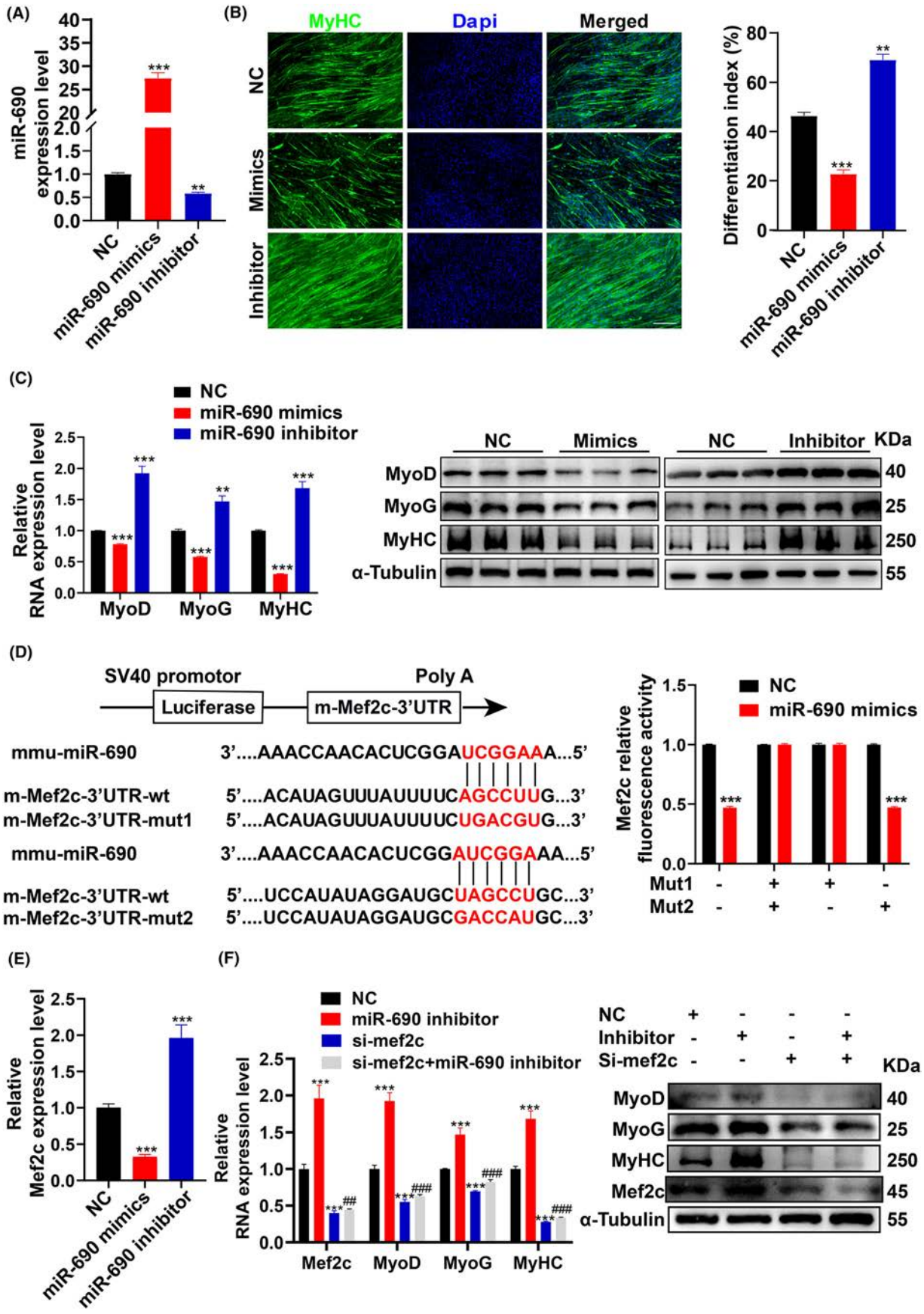

DOI: 10.1002/jcsm.13106

Figure 6 *MiR-690* inhibited C2C12 myoblast differentiation by targeting *Mef2c in vitro.* (A) Q-PCR analysis of *miR-690* level in C2C12 myoblast after transfection with *miR-690* mimics, *miR-690* inhibitors and negative control vehicle (NC) for 5 days, respectively. The *miR-690* overexpression level indicates the efficiency of *miR-690* mimics transfection. The *miR-690* down-regulated level indicates the efficiency of *miR-690* inhibitor transfection. (B) Left panel: The representative images of immunofluorescence staining for MyHC in C2C12 myoblasts after *miR-690* mimics, *miR-690* inhibitors and NC transfection, respectively. Scale bars, 200 μm. Right panel: The ratio of the MyHC-positive cell number to the total nuclei number as the differentiation index. (C) Left panel: Q-PCR analysis for the mRNA expression levels of myogenic marker genes, including *MyoD*, *MyoG* and *MyHC* during C2C12 myoblast differentiation after *miR-690* mimics, *miR-690* inhibitors and NC transfection, respectively. Right panel: Western blot analysis for the protein levels of myogenic markers, including MyoD, MyoG and MyHC, in C2C12 myoblast differentiation after treatment with *miR-690* mimics, *miR-690* inhibitors and NC, respectively. (D) Left panel: Diagram illustrating the construct of psiCHECK™-2 vector. The predicted binding sequence and its mutated sequences (Mut1, Mut2 and Mut1/2) at 3′-UTR of *Mef2c* by *miR-690* are highlighted. Right panel: The dual-luciferase reporter assay for fluorescent activity of MEF2C in HK293T cells after co-transfection with the WT or mutant Mef2c-3′-UTR luciferase construct in combination with *miR-690* mimics or NC. (E) Q-PCR analysis for the mRNA expression level of *Mef2c* in myoblasts after transfection with *miR-690* mimics, *miR-690* inhibitor and NC, respectively. (F) Left panel: Q-PCR analysis for the mRNA levels of *Mef2c*, *MyoD*, *MyoG* and *MyHC*, in C2C12 myoblasts after transfection with *miR-690* inhibitor, NC and si-*Mef2c* in combination with or without *miR-690* inhibitor for 5 days. Right panel: Western blot analysis for the protein levels of MyoD, MyoG, MyHC and Mef2c, in C2C12 myoblasts after transfection with *miR-690* inhibitor, negative control and si-*Mef2c* in combination with or without *miR-690* inhibitor for 5 days. Notes: Data are presented as means ± SEM. $^{*}P < 0.05$, $^{**}P < 0.01$, $^{***}P < 0.001$ vs. NC group by Student's *t*-test (A, B, C, D, E). $^{*}P < 0.05$, $^{**}P < 0.01$, $^{***}P < 0.001$ vs. NC group and $^{\#}P < 0.05$, $^{\#\#}P < 0.01$, $^{\#\#\#}P < 0.001$ vs. miR-690 inhibitor group by one-way ANOVA (F). *Mef2c*, muscle enhancer factors 2c; *MyHC*, muscle myosin heavy chain; *MyoD*, myoblast determination protein 1; *MyoG*, Myogenin.

expression of *Mef2c* during myoblast differentiation (*Figure* 6E). In addition, we transfected si-*Mef2c* and NC into C2C12 myoblasts. The results showed that the expression of *Mef2c* in vitro was significantly decreased by approximately fourfold compared with that in the NC group (*Figure* 6F). More importantly, we found that co-transfection of *si-Mef2c* and the *miR-690* inhibitor also significantly decreased the expression of myogenesis markers when compared with the *miR-690* inhibitor group (*Figure* 6F), indicating that *miR-690* mediates myogenesis by targeting *Mef2c*. Q-PCR and western blot analysis further indicated that *si-Mef2c* transfection in the presence or absence of *miR-690* inhibitors suppressed the expression of myogenesis-related genes, including Myod, Myog and Myhc, in myoblasts during differentiation **(***Figure* 6F**)**. Immunofluorescence staining of MYHC also demonstrated that myoblasts formed fewer myotubes after transfection with *si-Mef2c* or co-transfection with *si-Mef2c* and the *miR-690* inhibitor (*Figure* S5A). Taken together, these results suggest that *miR-690* directly targets Mef2c to inhibit C2C12 myoblast differentiation.

MiR-690 overexpression in TA muscle inhibited SCs myogenic capacity and induced muscle atrophy in vivo

To further examine the effect of *miR-690* on the myogenic capacity of SCs in vivo, we overexpressed *miR-690* in the TA muscle of adult mice using a recombinant AAV system, and an AAV vector encoding green fluorescent protein (GFP) was used to confirm that muscle injection with AAV was successful (*Figure* 7A). In mice injected with AAV-*miR-690*, the expression of *miR-690* increased 1.5-fold in TA muscle and interstitial sEVs from TA muscle, whereas the expression of *Mef2c* decreased in TA muscle (Figure 7B). Moreover, the immunofluorescence results showed that the number of $Pax7^{+}$ SCs (*Figure* S6A) and $Pax7^{+}MyoD^{+}$ cells (*Figure* 7C) was significantly reduced in TA muscle injected with AAV-*miR-690*, indicating decreased myogenic capacity of SCs. Interestingly, the expression levels of muscle atrophy-related genes atrogin-1 and murf-1 were significantly increased in mice injected with AAV-*miR-690* (*Figure* 7D). In addition, AAV-*miR-690*-treated TA muscle had a significantly smaller fibre CSA (*Figure* 7E). The maximum force generated by the EDL muscle was also suppressed after AAV-*miR-690* infection (*Figure* 7F). These data indicate that sEV *miR-690* inhibits the myogenic capacity of SCs and induces muscle atrophy.

Silencing miR-690 promoted SCs myogenic capacity and alleviated muscle atrophy in vivo

To test whether silencing *miR-690* expression in skeletal muscle could rescue the decreased myogenic capacity of SCs during ageing and counteract age-related muscle atrophy, we injected an AAV-9 vector expressing a *miR-690* sponge with GFP into the TA muscle of aged mice, which were sacrificed 4 weeks later (*Figure* 8A). In mice injected with AAV-*miR-690*-sponge, the expression of *miR-690* decreased by 80% in TA muscle and decreased by 40% in interstitial sEVs from TA muscle, whereas the expression of *Mef2c* increased by two-fold in TA muscle (*Figure* 8B). Moreover, the immunofluorescence results showed that the number of $Pax7^{+}$ SCs (*Figure S6B*) and $Pax7^{+}MyoD^{+}$ cells (*Figure* 8C) was significantly increased in TA muscle injected with AAV-*miR-690*-sponge, indicating enhanced myogenic capacity of SCs. Interestingly, the expression of muscle atrophy-related genes atrogin-1 and murf-1 were significantly decreased in mice injected with AAV-*miR-690*-sponge (*Figure* 8D). In addition, silencing *miR-690* expression in the TA muscle of aged mice alleviated the decline in fibre CSA during ageing (*Figure* 8E). The EDL muscle also generated a significantly higher maximal force in AAV-*miR-690* sponge mice than that in the AAV-control group (*Figure* 8F). These

DOI: 10.1002/jcsm.13106

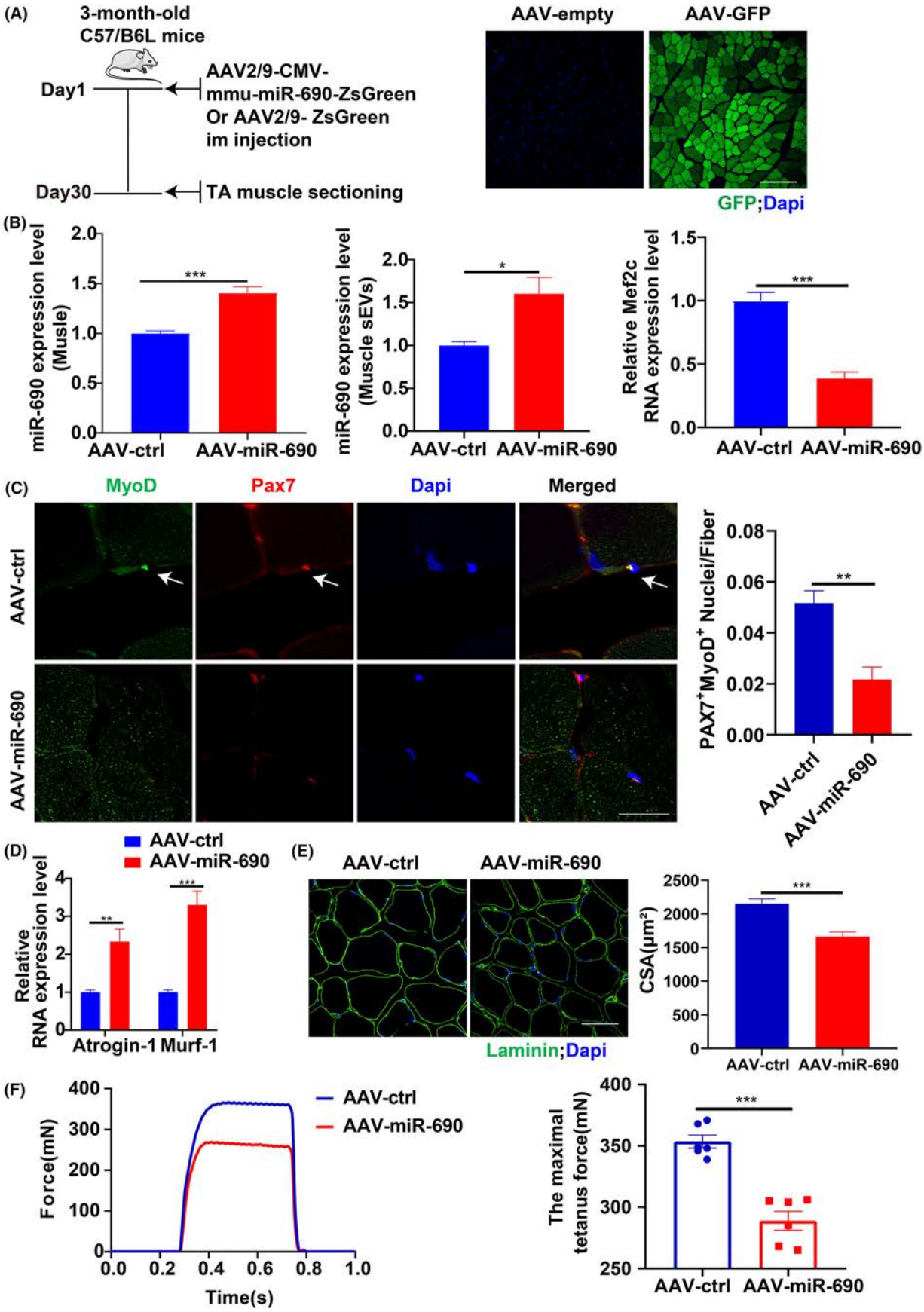

DOI: 10.1002/jcsm.13106

Figure 7 *MiR-690* overexpression in muscle fibres inhibited the myogenic capacity of SCs in vivo. (A) Left panel: Schematic diagram depicting the experimental design of administrating adult mice with recombinant AAV-*miR-690* via intramuscular injection in TA muscles. Right panel: The representative microscopy images of frozen cross sections from TA muscles transduced with AAV-empty (no insert in AAV expression vector) and AAV-GFP in TA muscles from adult mice. Fluorescence signals indicate the positive expression of green fluorescent protein (GFP, green) in muscle fibres. (B) Left panel: Q-PCR analysis of the *miR-690* expression level in TA muscles from AAV-ctrl mice and AAV-*miR-690* mice, respectively. Middle panel: Q-PCR analysis of the *miR-690* expression level in sEVs isolated from TA muscles of AAV-ctrl mice and AAV-*miR-690* mice, respectively. Right panel: Q-PCR analysis of the *Mef2c* expression level in TA muscles from AAV-ctrl mice and AAV-*miR-690* mice, respectively. (C) Left panel: The representative images of immunofluorescent staining for *Pax7* (red) and MyoD (green) in TA section from AAV-ctrl and AAV-*miR-690* mice. Nuclei were labelled by Dapi (blue). Scale bars, 50 μm. Right panel: The average number of $Pax7^{+}$ $MyoD^{+}$ cells per TA section from AAV-ctrl and AAV-*miR-690* mice, respectively. (D) Q-PCR analysis of the mRNA levels of muscle atrophy related markers including atrogin-1 and murf-1 expression in TA muscles from AAV-ctrl mice and AAV-*miR-690* mice, respectively. (E) Left panel: The representative images of immunofluorescent staining for laminin in cryosection of TA muscles from AAV-ctrl mice and AAV-*miR-690* mice, respectively. Scale bars, 100 μm. Right panel: Semi-quantitative analysis of fCSA in TA muscles from AAV-ctrl mice and AAV-*miR-690* mice, respectively. (F) Left panel: The representative curve of tetanic force generated by tetanic stimulation in EDL from AAV-ctrl and AAV-*miR-690* mice, respectively. Right panel: The maximal tetanic force of EDL muscle from AAV-ctrl and AAV-*miR-690* mice, respectively. Notes: Data are presented as means ± SEM. $*P < 0.05$, $**P < 0.01$, $***P < 0.001$ by Student's *t*-test. $N = 6$ for each group. EDL, extensor digitorum longus; fCSA, fibre cross-sectional area; TA, tibialis anterior.

data indicate that silencing *miR-690* promotes satellite cell myogenic capacity and ameliorates muscle atrophy during sarcopenia development.

Discussion

As a common and age-associated progressive skeletal muscle disorder, sarcopenia is characterized by atrophic muscle fibre and contractile dysfunction, which leads to a decreased quality of life and increased morbidity and mortality in elderly people.[2,21] Impaired satellite cell activity, including decreased proliferation and differentiation potential, occurs during ageing, which may contribute to impaired muscle regenerative capacity and muscle atrophy.[22,23] However, the mechanism underlying satellite cell dysfunction in sarcopenia remains unclear. In this study, we demonstrated that atrophic muscle fibre-derived sEV *miR-690* may inhibit satellite cell differentiation during ageing-induced muscle atrophy.

Several lines of evidence have shown that environmental factors from the circulatory system contribute to the ageing phenotype of SCs, as evidenced by the fact that exposure of aged SCs to a young systemic environment can rejuvenate part of satellite cell function.[24] Muscle fibres secrete a series of myokines/ sEVs to regulate metabolism in the muscle and extramuscular tissues in an autocrine/paracrine/endocrine manner during muscle atrophy.[4,25,26] It was also reported that myofibre-secreted sEVs that regulate myoblasts, such as myotube-derived sEVs, can promote the differentiation of myoblasts by altering the expression of cyclin D1 and myogenin.[27] However, it is still unclear whether myokines/ sEVs derived from muscle fibres affect SC activity during ageing-induced muscle atrophy. Here, we observed an interesting phenomenon in which sEVs released from atrophic myotubes could be transferred into myoblasts and subsequently inhibit myoblast differentiation in vitro. Furthermore, the injection of atrophic myotube-derived sEVs into the muscles of adult mice inhibited SCs differentiation. Moreover, administration of GW4869, a reversible inhibitor of neutral sphingomyelinase that prevents sEV generation, could increase the regenerative capacity of SCs. Taken together, sEVs released from myofibres can be transported into SCs and can inhibit SC differentiation during ageing.

Almost all aspects of skeletal muscle development and homoeostasis are regulated by miRNAs either directly or indirectly. Therefore, we employed RNA-seq analysis to examine the miRNA profiles of sEVs derived from control and atrophic myotubes. We identified *miR-690* as the most enriched miRNA among the 45 up-regulated miRNAs in sEVs released from atrophic myotubes. More importantly, *miR-690* in both muscle from aged mice tissue and muscle biopsies from sarcopenia patients increased, indicating that *miR-690* is the most important miRNA encapsulated in sEVs released from myofibres to affect SCs function during sarcopenia development. Previous studies have demonstrated that *miR-690* as a Runx2-targeted miRNA could regulate osteogenic differentiation of C2C12 myogenic progenitor cells by targeting NF-κB (p65),[28] indicating that *miR-690* may play important roles in Runx2-induced osteogenic differentiation. Importantly, *miR-690* was also reported to improve insulin sensitivity of adipose tissue, liver and skeletal muscle in obese mice as an exosome-derived miRNA from M2-polarized macrophages,[29] indicating that *miR-690* may play an important role in regulating energy metabolism in skeletal muscle. However, the pathophysiological role of *miR-690* in the regulation of SC differentiation in skeletal muscle remains unclear. In our study, we showed that *miR-690* overexpression inhibited myoblast differentiation in vitro, whereas *miR-690* inhibition led to the opposite effect. In addition, overexpression of *miR-690* can inhibit SCs myogenic capacity in the muscle tissue of adult mice, and vice versa. Thus, our findings suggest that *miR-690* encap-

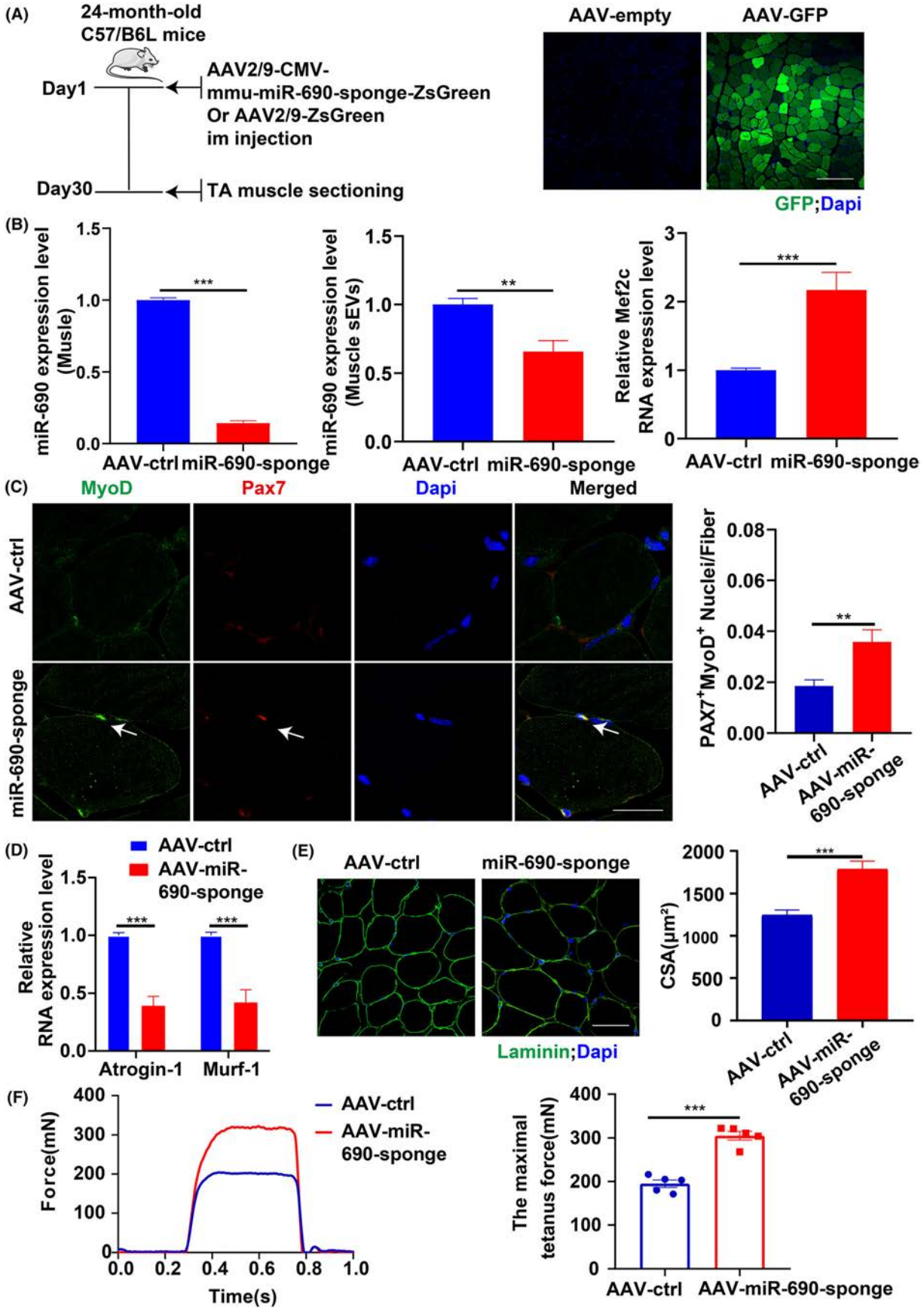

DOI: 10.1002/jcsm.13106

Figure 8 Silencing *miR-690* promoted SCs differentiation and alleviated muscle atrophy in aged mice. (A) Left panel: Schematic diagram illustrating the experimental design of administrating aged mice with recombinant AAV-*miR-690*-sponge via intramuscular injection in TA muscles. Right panel: The representative microscopy images of frozen cross sections from TA muscles transduced with AAV-empty (no insert in AAV expression vector) and AAV-GFP in TA muscles from aged mice. Fluorescence signals indicate the positive expression of green fluorescent protein (GFP, green) in muscle fibres. (B) Left panel: Q-PCR analysis for the expression level of *miR-690* in TA muscles of AAV-ctrl mice and AAV-*miR-690*-sponge mice, respectively. Middle panel: Q-PCR analysis for the expression level of *miR-690* in sEVs isolated from TA muscles of AAV-ctrl mice and AAV-*miR-690*-sponge mice, respectively. Right panel: Q-PCR analysis for the expression level of mef2c in TA muscles of AAV-ctrl mice and AAV-*miR-690*-sponge mice. (C) Left panel: The representative images of immunofluorescent staining for Pax7 (red) and MyoD (green) in TA section from AAV-ctrl and AAV-*miR-690*-sponge mice. Nuclei were labelled by DAPI (blue). Scale bars, 50 μm. Right panel: The average number of $Pax7^+$ $MyoD^+$ cells per TA section of AAV-ctrl and AAV-*miR-690*-sponge mice, respectively. (D) Q-PCR analysis for the expression levels of the muscle atrophy-related marker genes including atrogin-1 and murf-1 in TA muscles of AAV-ctrl mice and AAV-*miR-690*-sponge mice, respectively. (E) Left panel: The representative images of immunofluorescent staining for laminin in cryosection of TA muscles from AAV-ctrl mice and AAV-*miR-690*-sponge, respectively. Scale bars, 100 μm. Right panel: Semi-quantitative analysis for fCSA of TA muscle in AAV-ctrl mice and AAV-*miR-690*-sponge mice, respectively. (F) Left panel: The representative curve of tetanic force generated by tetanic stimulation in EDL from AAV-ctrl and AAV-*miR-690*-sponge mice, respectively. Right panel: The maximal tetanic force of EDL from AAV-ctrl and AAV-*miR-690*-sponge mice, respectively. Notes: Data are presented as means ± SEM. $^*P < 0.05$, $^{**}P < 0.01$, $^{***}P < 0.001$ by Student's *t*-test. $N = 6$ for group (B, C, D, E); $n = 5$ for group (F). EDL, extensor digitorum longus; fCSA, fibre cross-sectional area; TA, tibialis anterior.

sulated in sEVs released from myofibres negatively regulates SC differentiation.

Subsequently, we identified *Mef2c* as a major direct target of *miR-690*. *Mef2c* belongs to the myocyte enhancer factor 2 (*MEF2*) family of transcription factors, which are involved in multiple steps of skeletal muscle development, including myoblast differentiation and fusion, and various processes that regulate postnatal skeletal muscle homoeostasis and plasticity.[30,31] *Mef2c* also promotes muscle regeneration and re-growth after injury.[32] However, it has been documented that conditional deletion of individual *Mef2a*, *Mef2c* or *Mef2d* genes has no effect on mouse SCs in vivo, but combined conditional deletion of all three genes results in blocked regeneration.[33] The analysis indicated that this was because *Mef2c* is redundant with *Mef2a* and *Mef2d*. In our study, *Mef2c*, *Mef2a* and *Mef2d*, were identified as the target genes of *miR-690*, as evidenced by overexpression of *miR-690* decreased in the levels of *Mef2a*, *Mef2c* and *Mef2d* during myoblast differentiation. These results implied that *miR-690* may inhibit myoblast differentiation through the combined effects of *Mef2a*, *Mef2c* and *Mef2d*.

Recent studies have shown that depletion of SCs in adult sedentary mice impaired muscle regenerative capacity without affecting skeletal muscle myofibre size or composition.[34] Interestingly, we observed a decline in muscle fibre CSA and muscle strength as well as increased expression of the muscle atrophy markers *TRIM63/Murf1* and *FBXO32*/Atrogin-1 after overexpression of *miR-690* in the muscle tissue of adult mice. Our data suggest that *miR-690* overexpression not only inhibits SCs myogenic capacity but also induces muscle atrophy in adult mice. Therefore, we speculated that this may be due to the reduced expression of *Mef2c*, which is a well-established modulator of myofibre homoeostasis and hypertrophy.[35] *Mef2c* also plays an important role in the integrity and maintenance.[36] Additional studies have demonstrated that denervation atrophy can be inhibited by activated *MEF2*[35] and that *MEF2* can restore fibre size in atrophic muscles of adult spinal and bulbar muscular atrophy mice.[37] Decreased MEF2C protein expression can also cause type I muscle atrophy under microgravity,[38] and MEF2C can significantly block cancer-induced muscle wasting and dysfunction.[39] Supporting this notion, activin A causes cancer-induced muscle atrophy by inhibiting *MyHC-β*/slow synthesis through the down-regulation of MEF2C.[40] Taken together, these studies have established that *Mef2c* plays an important role in muscle atrophy.

In summary, our findings demonstrate that atrophic muscle fibre-derived sEV *miR-690* may inhibit SCs myogenic capacity by targeting *MEF2* during ageing (*Figure* S7). sEV-mediated intercellular communication between muscle fibres and SCs enriches our understanding of SC number and myogenic capacity during ageing-induced muscle atrophy. Moreover, *miR-690* may be a novel therapeutic target for restoring the myogenic capacity of SCs in aged mice, augmenting muscle mass and strength and overcoming sarcopenia.

Acknowledgements

The authors certify that they complied with the ethical guidelines for publishing in the *Journal of Cachexia, Sarcopenia and Muscle*.[41]

Funding

This work was supported by research grants from the National Key Research and Development Program of China (2020YFC2004900); Youth Thousand Talents Program of China (13004001); National Science Foundation of China (82272530, 81991514, 82002370, 82000069 and 81972124); Natural Science Foundation of Jiangsu Province of China (BK20200314 and BK20200117); The Research Team

Start-up Funds of Nanjing University (14912203); Jiangsu Provincial Key Medical Center Foundation; Jiangsu Provincial Medical Outstanding Talent Foundation; Jiangsu Provincial Medical Youth Talent Foundation; Jiangsu Provincial Key Medical Talent Foundation; Program of Innovation and Entrepreneurship of Jiangsu Province; The Fundamental Research Funds for the Central Universities (14380493 and 14380494); Jiangsu postdoctoral research support project (2021K059A); China Postdoctoral Science Foundation (2019M661806); and Postgraduate Research & Practice Innovation Program of Jiangsu Province.

Conflict of interest

The authors disclose no potential conflicts of interest.

Online supplementary material

Additional supporting information may be found online in the Supporting Information section at the end of the article.

References

1. Mayhew AJ, Amog K, Phillips S, Parise G, McNicholas PD, de Souza RJ, Thabane L, Raina P. The prevalence of sarcopenia in community-dwelling older adults, an exploration of differences between studies and within definitions: A systematic review and meta-analyses. *Age Ageing* 2019;**48**: 48–56.
2. Cruz-Jentoft AJ, Bahat G, Bauer J, Boirie Y, Bruyère O, Cederholm T, Cooper C, Landi F, Rolland Y, Sayer AA, Schneider SM, Sieber CC, Topinkova E, Vandewoude M, Visser M, Zamboni M, Writing Group for the European Working Group on Sarcopenia in Older People 2 (EWGSOP2), and the Extended Group for EWGSOP2, Bautmans I, Baeyens JP, Cesari M, Cherubini A, Kanis J, Maggio M, Martin F, Michel JP, Pitkala K, Reginster JY, Rizzoli R, Sánchez-Rodríguez D, Schols J. Sarcopenia: Revised European consensus on definition and diagnosis. *Age Ageing* 2019;**48**:16–31.
3. Beaudart C, Zaaria M, Pasleau F, Reginster JY, Bruyere O. Health outcomes of sarcopenia: A systematic review and meta-analysis. *PLoS ONE* 2017;**12**:e0169548.
4. Siriett V, Salerno MS, Berry C, Nicholas G, Bower R, Kambadur R, Sharma M. Antagonism of myostatin enhances muscle regeneration during sarcopenia. *Mole Ther:J Am Soc Gene Ther* 2007;**15**:1463–1470.
5. Lees SJ, Rathbone CR, Booth FW. Age-associated decrease in muscle precursor cell differentiation. *Am J Physiol Cell Physiol* 2006;**290**:C609–C615.
6. Seale P, Sabourin LA, Girgis-Gabardo A, Mansouri A, Gruss P, Rudnicki MA. Pax7 is required for the specification of myogenic satellite cells. *Cell* 2000;**102**:777–786.
7. Kuang S, Gillespie MA, Rudnicki MA. Niche regulation of muscle satellite cell self-renewal and differentiation. *Cell Stem Cell* 2008;**2**:22–31.
8. Rozo M, Li L, Fan CM. Targeting beta1-integrin signaling enhances regeneration in aged and dystrophic muscle in mice. *Nat Med* 2016;**22**:889–896.
9. Zhang C, Cheng N, Qiao B, Zhang F, Wu J, Liu C, Li Y, Du J. Age-related decline of interferon-gamma responses in macrophage impairs satellite cell proliferation and regeneration. *J Cachexia Sarcopenia Muscle* 2020;**11**:1291–1305.
10. Lee JH, Jun HS. Role of myokines in regulating skeletal muscle mass and function. *Front Physiol* 2019;**10**:42.
11. Reza MM, Subramaniyam N, Sim CM, Ge X, Sathiakumar D, McFarlane C, Sharma M, Kambadur R. Irisin is a pro-myogenic factor that induces skeletal muscle hypertrophy and rescues denervation-induced atrophy. *Nat Commun* 2017;**8**:1104.
12. Izumiya Y, Bina HA, Ouchi N, Akasaki Y, Kharitonenkov A, Walsh K. FGF21 is an Akt-regulated myokine. *FEBS Lett* 2008; **582**:3805–3810.
13. Murphy C, Withrow J, Hunter M, Liu Y, Tang YL, Fulzele S, Hamrick MW. Emerging role of extracellular vesicles in musculoskeletal diseases. *Mol Aspects Med* 2018;**60**: 123–128.
14. Kalluri R, LeBleu VS. The biology, function, and biomedical applications of exosomes. *Science (New York, NY)* 2020;**367**.
15. Braun T, Gautel M. Transcriptional mechanisms regulating skeletal muscle differentiation, growth and homeostasis. *Nat Rev Mol Cell Biol* 2011;**12**:349–361.
16. Wu L, Belasco JG. Let me count the ways: Mechanisms of gene regulation by miRNAs and siRNAs. *Mol Cell* 2008;**29**:1–7.
17. Forterre A, Jalabert A, Berger E, Baudet M, Chikh K, Errazuriz E, de Larichaudy J, Chanon S, Weiss-Gayet M, Hesse AM, Record M, Geloen A, Lefai E, Vidal H, Couté Y, Rome S. Proteomic analysis of C2C12 myoblast and myotube exosome-like vesicles: A new paradigm for myoblast-myotube cross talk? *PLoS ONE* 2014;**9**: e84153.
18. De Gasperi R, Hamidi S, Harlow LM, Ksiezak-Reding H, Bauman WA, Cardozo CP. Denervation-related alterations and biological activity of miRNAs contained in exosomes released by skeletal muscle fibers. *Sci Rep* 2017;**7**:12888.
19. Crewe C, Joffin N, Rutkowski JM, Kim M, Zhang F, Towler DA, Gordillo R, Scherer PE. An endothelial-to-adipocyte extracellular vesicle axis governed by metabolic state. *Cell* 2018;**175**:695–708 e13.
20. Yang CP, Yang WS, Wong YH, Wang KH, Teng YC, Chang MH, Liao KH, Nian FS, Chao CC, Tsai JW, Hwang WL, Lin MW, Tzeng TY, Wang PN, Campbell M, Chen LK, Tsai TF, Chang PC, Kung HJ. Muscle atrophy-related myotube-derived exosomal microRNA in neuronal dysfunction: Targeting both coding and long noncoding RNAs. *Aging Cell* 2020;**19**:e13107.
21. Mitchell WK, Williams J, Atherton P, Larvin M, Lund J, Narici M. Sarcopenia, dynapenia, and the impact of advancing age on human skeletal muscle size and strength; A quantitative review. *Front Physiol* 2012;**3**:260.
22. Sousa-Victor P, Gutarra S, García-Prat L, Rodriguez-Ubreva J, Ortet L, Ruiz-Bonilla V, Jardí M, Ballestar E, González S, Serrano AL, Perdiguero E, Muñoz-Cánoves P. Geriatric muscle stem cells switch reversible quiescence into senescence. *Nature* 2014; **506**:316–321.
23. Jang YC, Sinha M, Cerletti M, Dall'Osso C, Wagers AJ. Skeletal muscle stem cells: Effects of aging and metabolism on muscle regenerative function. *Cold Spring Harb Symp Quant Biol* 2011;**76**:101–111.
24. Conboy IM, Conboy MJ, Wagers AJ, Girma ER, Weissman IL, Rando TA. Rejuvenation of aged progenitor cells by exposure to a young systemic environment. *Nature* 2005;**433**:760–764.
25. Barbalho SM, Flato UAP, Tofano RJ, Goulart RA, Guiguer EL, Detregiachi CRP, Buchaim DV, Araújo AC, Buchaim RL, Reina FTR, Biteli P, Reina DOBR, Bechara MD. Physical exercise and myokines: Relationships with sarcopenia and cardiovascular complications. *Int J Mol Sci* 2020;**21**.
26. Rome S, Forterre A, Mizgier ML, Bouzakri K. Skeletal muscle-released extracellular vesicles: State of the art. *Front Physiol* 2019;**10**:929.
27. Forterre A, Jalabert A, Chikh K, Pesenti S, Euthine V, Granjon A, Errazuriz E, Lefai E, Vidal H, Rome S. Myotube-derived exosomal miRNAs downregulate Sirtuin1 in myoblasts during muscle cell differentiation. *Cell Cycle* 2014;**13**:78–89.
28. Yu S, Geng Q, Pan Q, Liu Z, Ding S, Xiang Q, Sun F, Wang C, Huang Y, Hong A. MiR-690,

a Runx2-targeted miRNA, regulates osteogenic differentiation of C2C12 myogenic progenitor cells by targeting NF-kappaB p65. *Cell Biosci* 2016;**6**:10.
29. Ying W, Gao H, dos Reis FCG, Bandyopadhyay G, Ofrecio JM, Luo Z, Ji Y, Jin Z, Ly C, Olefsky JM. MiR-690, an exosomal-derived miRNA from M2-polarized macrophages, improves insulin sensitivity in obese mice. *Cell Metab* 2021;**33**:781–790.e5.
30. Potthoff MJ, Olson EN. MEF2: A central regulator of diverse developmental programs. *Development* 2007;**134**: 4131–4140.
31. Mokalled MH, Johnson AN, Creemers EE, Olson EN. MASTR directs MyoD-dependent satellite cell differentiation during skeletal muscle regeneration. *Genes Dev* 2012;**26**: 190–202.
32. Baruffaldi F, Montarras D, Basile V, de Feo L, Badodi S, Ganassi M, Battini R, Nicoletti C, Imbriano C, Musarò A, Molinari S. Dynamic phosphorylation of the myocyte enhancer factor 2Cα1 splice variant promotes skeletal muscle regeneration and hypertrophy. *Stem cells (Dayton, Ohio)* 2017;**35**: 725–738.
33. Liu N, Nelson BR, Bezprozvannaya S, Shelton JM, Richardson JA, Bassel-Duby R, Olson EN. Requirement of MEF2A, C, and D for skeletal muscle regeneration. *Proc Natl Acad Sci U S A* 2014;**111**:4109–4114.
34. Fry CS, Lee JD, Mula J, Kirby TJ, Jackson JR, Liu F, Yang L, Mendias CL, Dupont-Versteegden EE, McCarthy JJ, Peterson CA. Inducible depletion of satellite cells in adult, sedentary mice impairs muscle regenerative capacity without affecting sarcopenia. *Nat Med* 2015;**21**:76–80.
35. Moretti I, Ciciliot S, Dyar KA, Abraham R, Murgia M, Agatea L, Akimoto T, Bicciato S, Forcato M, Pierre P, Uhlenhaut NH, Rigby PWJ, Carvajal JJ, Blaauw B, Calabria E, Schiaffino S. MRF4 negatively regulates adult skeletal muscle growth by repressing MEF2 activity. *Nat Commun* 2016;**7**:12397.
36. Potthoff MJ, Arnold MA, McAnally J, Richardson JA, Bassel-Duby R, Olson EN. Regulation of skeletal muscle sarcomere integrity and postnatal muscle function by Mef2c. *Mol Cell Biol* 2007;**27**:8143–8151.
37. Nath SR, Lieberman ML, Yu Z, Marchioretti C, Jones ST, Danby ECE, van Pelt K, Sorarù G, Robins DM, Bates GP, Pennuto M, Lieberman AP. MEF2 impairment underlies skeletal muscle atrophy in polyglutamine disease. *Acta Neuropathol* 2020;**140**: 63–80.
38. Yamakuchi M, Higuchi I, Masuda S, Ohira Y, Kubo T, Kato Y, Maruyama I, Kitajima I. Type I muscle atrophy caused by microgravity-induced decrease of myocyte enhancer factor 2C (MEF2C) protein expression. *FEBS Lett* 2000;**477**:135–140.
39. Judge SM, Deyhle MR, Neyroud D, Nosacka RL, D'Lugos AC, Cameron ME, Vohra RS, Smuder AJ, Roberts BM, Callaway CS, Underwood PW, Chrzanowski SM, Batra A, Murphy ME, Heaven JD, Walter GA, Trevino JG, Judge AR. MEF2c-dependent downregulation of myocilin mediates cancer-induced muscle wasting and associates with cachexia in patients with cancer. *Cancer Res* 2020;**80**:1861–1874.
40. Loumaye A, Lause P, Zhong X, Zimmers TA, Bindels LB, Thissen JP. Activin A causes muscle atrophy through MEF2C-dependent impaired myogenesis. *Cell* 2022;**11**:1119.
41. von Haehling S, Morley JE, Coats AJS, Anker SD. Ethical guidelines for publishing in the Journal of Cachexia, Sarcopenia and Muscle: Update 2021. *J Cachexia Sarcopenia Muscle* 2021;**12**:2259–2261.